Discrete dislocation and nonlocal crystal plasticity modelling

Yefimov, Serge

Chapter 6

Size effects in single crystal thin films: nonlocal crystal plasticity simulations

Abstract

Stress relaxation in single crystalline thin films on substrates subjected to thermal loading is studied using the nonlocal continuum crystal plasticity theory proposed in the previous chapter. The theory is founded on a statistical-mechanics description of the collective behavior of dislocations in multiple slip, which is coupled to a small-strain continuum crystal plasticity formulation. The theory is inherently nonlocal with the length scale being determined by the evolving dislocation density. Symmetric double slip is considered while the film is in plane strain. The predicted stress versus temperature response and the evolution of the dislocation structure are analyzed for different orientations and film thicknesses. The effect of film size is associated with the formation of a boundary layer of dislocations at the film-substrate interface which does not scale with the film thickness. The width of the boundary layer itself is shown to be dependent on the slip system orientation. The results are consistent with those of recent discrete dislocation simulations.

6.1 Introduction

The continuing demand in modern high-tech industries is the development of smaller and smaller devices for various applications in microelectronics, communication technology, optical electronics, Micro-Electro-Mechanical Systems (MEMS) etc. Thin films having thickness of a few microns or even a fraction of a micron are commonly used as components in MEMS and in microelectronic devices. Successful industrial implementation of thin films requires knowledge of their mechanical properties. The mechanical properties of thin films are different from those of their bulk counterparts because of their unique microstructure, reduced dimensions and the constraints imposed by the substrate.

During thermal excursions in processing steps or in service, large stresses can develop in the thin films as a result of the difference between the thermal expansion coefficient of the films and the (semiconductor) substrates. It has been observed that as the thickness of a thin crystalline film decreases, the stress that is built up increases. Figure 6.1 shows a typical size dependent stress-temperature response for thin films under thermal cycling, which was obtained experimentally by Leung *et al.* (2000) for bare and passivated gold films on a silicon substrate using the wafer curvature technique. Upon cooling a film from an almost stress-free state at a relatively high temperature, the deformation is initially elastic, but as cooling proceeds plastic deformation eventually occurs. Stress relaxation is apparently less efficient in thinner films, where the resulting stress levels are higher than in thicker films, cf. Fig. 6.1(b) with 6.1(a). When the film is re-heated, the stress level in the film at first reduces (in absolute value) elastically, with reverse plastic deformation subsequently occurring for a sufficiently large temperature change. Reverse plastic deformation occurs earlier and stress levels increase more rapidly for thinner films. These effects have been observed for fine and coarse-grained

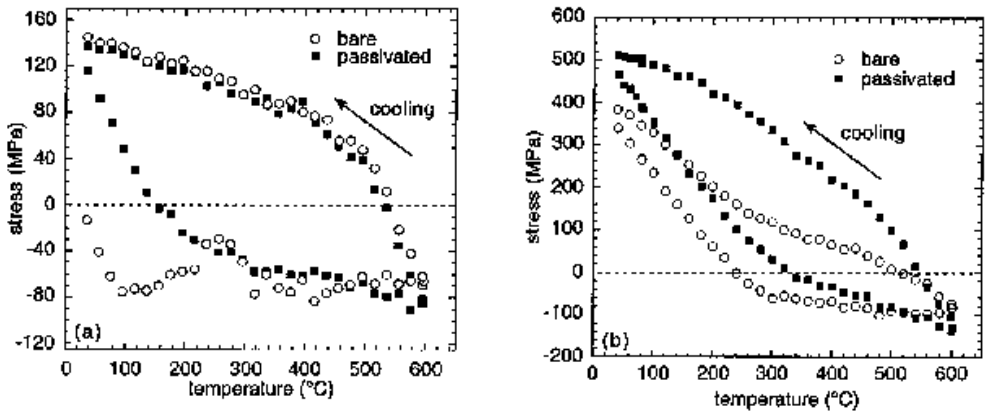

Figure 6.1 Stress relaxation in thin gold films upon cooling. (a) film thickness of 0.75μm; (b) 0.5μm. (from Leung *et al.*, 2000).

films as well as for single crystalline films. We will confine our attention here to single crystalline films to avoid the grain-size effect that complicates matters significantly.

The size-dependent plastic deformation in micron-scale films is primarily caused by the dimensional constraints of the films (Arzt, 1998). However, classical local plasticity theories are insensitive to such constraints due to lack of a material length scale. Various dislocation based arguments have been put forward to explain the size dependence. The most successfull of these is the single dislocation model proposed by Freund (1987) and Nix (1998) based on the confined motion of a threading dislocation in a single crystal film, which suggests that the yield strength scales with the film thickness h as h^{-1}.

To study the problem of stress relaxation in single crystalline thin films on a substrates subjected to thermal loading, the nonlocal crystal plasticity model developed in the previous chapters is used. The numerical results of the problem are compared with those of a discrete dislocation study by Nicola *et al.* (2003a). There it has been found that the effect of film size is associated with the formation of a boundary layer of piled-up dislocations at the film-substrate interface. One aim of our study is to see if this is recovered by our nonlocal continuum theory. A similar comparison has been carried out by Nicola *et al.* (2004b) with the nonlocal theory of Gurtin (2002).

6.2 Problem formulation

We consider a two-dimensional representation of a metallic single-crystalline thin film that is perfectly bonded to an infinitely large elastic substrate, as sketched in Fig. 6.2, and has a free surface at the top. A Cartesian coordinate system is used with the x_1-axis parallel to the film-substrate interface and x_2 in the thickness direction. The film-substrate system is subject to thermal expansion with a prescribed constant temperature rate $\dot{T}$ while maintaining plane strain conditions in the out-of-plane direction. The film has a thickness of h and is assumed to have two slip systems. The slip systems are oriented at an angle $\varphi^{(\beta)}$ ($\beta = 1,2$) with respect to the x_1 axis and are defined by pairs of unit vectors $(\boldsymbol{s}^{(\beta)}, \boldsymbol{m}^{(\beta)})$ in the direction of slip and the slip plane normal, respectively. The film-substrate interface is taken to be impenetrable for the dislocations, so that the substrate remains elastic. The linear thermal expansion coefficients of the film and the substrate are denoted by α_f and α_s, respectively, with $\alpha_s < \alpha_f$ for typical systems of metallic films on a Si substrate. Young's modulus E and Poisson ratio ν are taken to be identical for the film and the substrate. Ovecoglu *et al.* (1987) have shown that the difference in the elastic properties between film and substrate does not qualitatively change the dislocation motion. Thus, the thermal stress that builds up in the system is solely caused by the constrained thermal expansion due to the difference between α_f and α_s. Because of this, and since we are interested only in the stress relaxation, the original problem in Fig. 6.2 can be replaced with the problem depicted in Fig. 6.3a, where the film is subject to thermal expansion with thermal expansion coefficient $\alpha = \alpha_f - \alpha_s$, while the substrate does not expand (as in the discrete dislocation simulations of Nicola *et al.*, 2003a). Moreover, since we are aiming to

study only plasticity in the film and the substrate is very large, the substrate can be removed from the consideration (see Fig. 6.3b), and its role replaced approximately by the boundary conditions at the bottom of the film:

$$u_1 = 0, \quad u_2 = 0 \quad \text{along } x_2 = 0. \tag{6.1}$$

This is equivalent to assuming the substrate to be rigid and this ignores the small amount of deformation in the top layer of the substrate; the findings in Nicola et al. (2003a) suggest that these effects are negligible. At the top surface of the film traction-free boundary conditions are imposed,

$$\sigma_{12} = 0, \quad \sigma_{22} = 0 \quad \text{along } x_2 = h. \tag{6.2}$$

We take the film to be infinitely long but periodic with a period of L, so that only a unit cell of width L (see Fig. 6.3b) needs to be analyzed with the following periodic boundary conditions

$$u_1(0,x_2) = u_1(L,x_2) \quad \text{and} \quad u_2(0,x_2) = u_2(L,x_2). \tag{6.3}$$

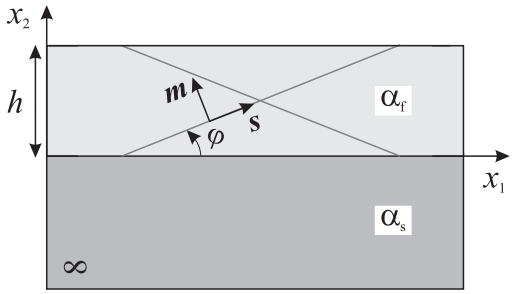

Figure 6.2 Sketch of the problem: a single crystal thin film bonded to a half-infinite elastic substrate. ***s*** and ***m*** are unit vectors denoting the slip direction and the slip plane normal, respectively.

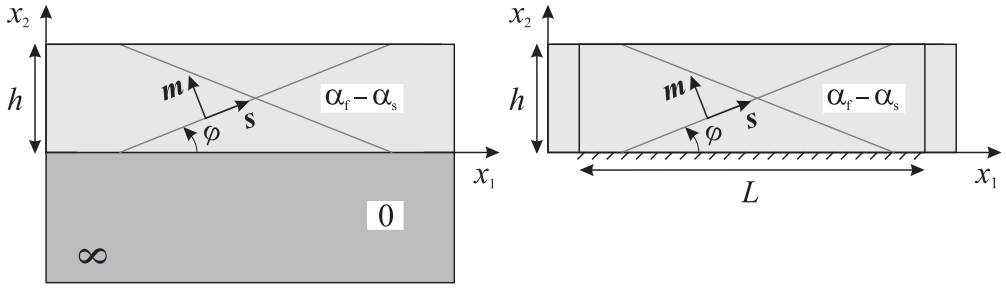

(a) (b)

Figure 6.3 (a) Simplified problem formulation with the uniform thermal expansion separated off; (b) Unit cell of the thin film with width L as it is actually analyzed.

6.3 Summary of the constitutive theory

The nonlocal crystal plasticity formulation proposed in Yefimov and Van der Giessen (2004c) is used to solve the boundary value problem. The theory was originally developed for single slip (Yefimov *et al.*, 2004a). It is based on a statistical-mechanics description of the collective behavior of dislocations in two dimensions, and comprises two coupled parts: a continuum dislocation dynamics and the small-strain framework of single crystal continuum plasticity (see, e.g., Asaro, 1983). The extension to multiple slip adopted here was proposed by Yefimov and Van der Giessen (2004c). The continuum dislocation dynamics in multiple slip is defined by the following set of transport equations for the total dislocation density $\rho^{(\beta)}$ on a slip system β and for the net Burgers-vector dislocation density $k^{(\beta)}$:

$$\frac{\partial \rho^{(\beta)}}{\partial t} + \frac{\partial}{\partial \boldsymbol{r}} \cdot (k^{(\beta)} \boldsymbol{v}^{(\beta)}) = f^{(\beta)}, \tag{6.4}$$

$$\frac{\partial k^{(\beta)}}{\partial t} + \frac{\partial}{\partial \boldsymbol{r}} \cdot (\rho^{(\beta)} \boldsymbol{v}^{(\beta)}) = 0. \tag{6.5}$$

Here, $\boldsymbol{v}^{(\beta)}$ is the average continuum dislocation glide velocity and is defined as

$$\boldsymbol{v}^{(\beta)} = B^{-1} \boldsymbol{b}^{(\beta)} (\tau^{(\beta)} - \tau_{\text{tot}}^{(\beta)}), \tag{6.6}$$

where B is the dislocation drag coefficient and $\boldsymbol{b}^{(\beta)}$ is the Burgers vector of the dislocations on slip system β. $\tau^{(\beta)} = \boldsymbol{m}^{(\beta)} \cdot \boldsymbol{\sigma} \cdot \boldsymbol{s}^{(\beta)}$ and $\tau_{\text{tot}}^{(\beta)}$ are the resolved shear stress and the total backstress on slip system β, respectively. The latter is given by

$$\tau_{\text{tot}}^{(\beta)} = \sum_{\zeta} S^{(\beta\zeta)} \tau_{\text{s}}^{(\zeta)}, \tag{6.7}$$

with $S^{(\beta\zeta)}$ being a projection matrix and $\tau_{\text{s}}^{(\zeta)}$ the self back stress from the single slip approximation (Yefimov *et al.*, 2004a),

$$\tau_{\text{s}}^{(\zeta)} = \frac{\mu \boldsymbol{b}^{(\zeta)}}{2\pi(1-\nu)\rho^{(\zeta)}} \cdot D \frac{\partial k^{(\zeta)}}{\partial \boldsymbol{r}}. \tag{6.8}$$

The nondimensional coefficient D enters through consideration of the dislocation-dislocation correlation functions (Groma *et al.*, 2003) and is of order unity. The projection matrix $S^{(\beta\zeta)}$ governs the nonlocal interactions between the dislocations on different slip systems and we take it to have the form

$$S^{(\beta\zeta)} = \boldsymbol{m}^{(\beta)} \cdot \left[\boldsymbol{s}^{(\zeta)} \otimes \boldsymbol{m}^{(\zeta)} + \boldsymbol{m}^{(\zeta)} \otimes \boldsymbol{s}^{(\zeta)} \right] \cdot \boldsymbol{s}^{(\beta)}. \tag{6.9}$$

The production term $f^{(\beta)}$ in Eq. (6.4) is given by

$$f^{(\beta)} = C^{(\beta)} \rho_{\text{nuc}}^{(\beta)} |\tau^{(\beta)} - \tau_{\text{tot}}^{(\beta)}| - A L_e (\rho^{(\beta)} + k^{(\beta)})(\rho^{(\beta)} - k^{(\beta)}) |\boldsymbol{v}^{(\beta)}|. \tag{6.10}$$

The first term in the right hand side represents dislocation nucleation from sources at a density $\rho_{\rm nuc}^{(\beta)}$, with the parameter $C^{(\beta)}$ being defined by

$$C^{(\beta)} = \frac{1}{\tau_{\rm nuc} t_{\rm nuc}} \text{ if } |\tau^{(\beta)} - \tau_{\rm tot}^{(\beta)}| \geq \tau_{\rm nuc}; \quad C^{(\beta)} = 0 \text{ otherwise.} \tag{6.11}$$

The second term controls the annihilation of the opposite sign dislocations on the same slip system, where A is a dimensionless parameter and L_e is the annihilation distance.

The continuum dislocation dynamics, governed by Eqs. (6.4)–(6.11), is coupled to a single crystal plasticity framework as follows. The plastic strain rate $\dot{\boldsymbol{\varepsilon}}^{\rm p}$ is determined in the usual way (e.g. Asaro, 1983) by the slip rates $\dot{\gamma}^{(\beta)}$ according to

$$\dot{\boldsymbol{\varepsilon}}^{\rm p} = \sum_{\beta} \dot{\gamma}^{(\beta)} \boldsymbol{P}^{(\beta)}, \tag{6.12}$$

where $\boldsymbol{P}^{(\beta)}$ is the Schmid orientation tensor given by

$$\boldsymbol{P}^{(\beta)} = \tfrac{1}{2}\left[\boldsymbol{s}^{(\beta)} \otimes \boldsymbol{m}^{(\beta)} + \boldsymbol{m}^{(\beta)} \otimes \boldsymbol{s}^{(\beta)}\right]. \tag{6.13}$$

The slip rate $\dot{\gamma}^{(\beta)}$ is, in turn, linked to the dislocation glide velocity $\boldsymbol{v}^{(\beta)}$ from Eq. (6.6) through the Orowan relation

$$\dot{\gamma}^{(\beta)} = \rho^{(\beta)} \boldsymbol{b}^{(\beta)} \cdot \boldsymbol{v}^{(\beta)}.$$

The thermo-elastic constitutive relation is specified in rate form as

$$\dot{\boldsymbol{\sigma}} = \boldsymbol{\mathcal{L}} : \dot{\boldsymbol{\varepsilon}}^{\rm e} - \frac{E}{1-2\nu}\alpha \dot{T} \boldsymbol{I}, \tag{6.14}$$

where $\boldsymbol{\mathcal{L}}$ is the isotropic elastic modulus tensor,

$$\mathcal{L}_{ijkl} = \frac{E}{1+\nu}\left[\tfrac{1}{2}\left(\delta_{ik}\delta_{jl} + \delta_{il}\delta_{jk}\right) + \tfrac{\nu}{1-2\nu}\delta_{ij}\delta_{kl}\right],$$

in terms of Young's modulus E and Poisson's ratio ν, and $\boldsymbol{I}$ is the unit tensor. The total strain is $\boldsymbol{\varepsilon} = \boldsymbol{\varepsilon}^{\rm e} + \boldsymbol{\varepsilon}^{\rm p}$.

We also stipulate the material response to be elastic ($\dot{\gamma}^{(\beta)} = 0$) unless $|\tau^{(\beta)} - \tau_{\rm tot}^{(\beta)}| > \tau_{\rm res}$. The introduction of this slip resistance $\tau_{\rm res}$ is a phenomenological fix to the dislocation dynamics discussed in Yefimov *et al.* (2004a) for reversal of the direction of dislocation motion.

In addition to purely mechanical boundary conditions (6.1)-(6.3), the theory requires additional boundary conditions for the dislocation dynamics part. Along the lateral sides $x_1 = 0$ and $x_1 = L$ of the unit cell, periodic boundary conditions are applied, so that $\rho^{(\beta)}(L, x_2) = \rho^{(\beta)}(0, x_2)$ and $k^{(\beta)}(L, x_2) = k^{(\beta)}(0, x_2)$ at all times. At the bottom of the film we model an impenetrable wall for the dislocations, consistent with the discrete dislocation calculations of Nicola *et al.*, 2003a). Thus, we require the dislocation velocity component normal to the boundary to vanish, i.e.

$$\boldsymbol{v}^{(\beta)} \cdot \boldsymbol{n} = 0 \quad \text{along } x_1 = 0, \tag{6.15}$$

where $\boldsymbol{n}$ is the unit normal to the bottom surface. At the top of the film where the macroscopic free surface condition (6.2) is applied, a natural dislocation outflow may occur. We assume the dislocations leave the domain with no reflection from the surface at $x_2 = h$ and apply no essential boundary condition at the outflow boundary. The same natural boundary condition has been adopted in previous studies of the bending of a single crystal strip (Yefimov *et al.*, 2004b, c).

The numerical implementation of the nonlocal crystal plasticity model uses the standard finite element method, as reported in detail by Yefimov *et al.* (2004a) for another boundary value problem. The dislocation dynamics part of the problem and the crystal plasticity part are solved incrementally in a staggered manner. An explicit time integration scheme is used with the same time steps for both subproblems. The spatial discretization is based on quadrilateral elements consisting of four crossed linear triangular elements. The two meshes for the two subproblems are taken to be identical for convenient passing of information.

The finite element analysis of the crystal plasticity part is based on a Lagrangian formulation of the field equations and the rate principle of virtual work

$$\int_V \dot{\boldsymbol{\sigma}} : \delta\dot{\boldsymbol{\varepsilon}}\, dV = \int_S \dot{\boldsymbol{T}} \cdot \delta\dot{\boldsymbol{u}}\, dS, \tag{6.16}$$

where V and S are the volume and surface of the body in the reference configuration, respectively, $\boldsymbol{n}^*$ is the unit outer normal to S, and

$$\varepsilon_{ij} = \frac{1}{2}\left(\frac{\partial u_i}{\partial x_j} + \frac{\partial u_j}{\partial x_i}\right), \quad T_i = \sigma_{ij} n_j^*. \tag{6.17}$$

The associated boundary conditions have already been given in (6.1–6.3).

The spatial discretization of the dislocation dynamics part is based on the interpolation of $\rho^{(\beta)}$ and $k^{(\beta)}$ density fields. Inside each finite element, these fields are expressed via the nodal values according to

$$\rho^{(\beta)} = \mathbf{N}^T \boldsymbol{\rho}^{(\beta)}, \tag{6.18}$$

$$k^{(\beta)} = \mathbf{N}^T \boldsymbol{k}^{(\beta)}, \tag{6.19}$$

where $\boldsymbol{\rho}^{(\beta)}$ and $\boldsymbol{k}^{(\beta)}$ are the vectors of nodal values of the dislocation densities $\rho^{(\beta)}$ and $k^{(\beta)}$, respectively. $\mathbf{N}$ is the vector of C_0 continuous shape functions. As a consequence, $\rho^{(\beta)}$ and $k^{(\beta)}$ are continuous across the element boundaries, while their derivatives are not. Therefore, the back stresses, cf. Eq. (6.8), are governed by a lower-dimensional interpolation and defined at the integration points of elements, just like the resolved shear stress $\tau^{(\beta)}$. Further details on weighted-residual Galerkin method implementation for the dislocation dynamics part can be found in Yefimov *et al.* (2004a).

6.4 Results

Most of the results to be presented here are for a film with a thickness of $h = 1\,\mu$m, and we will study size effects in a separate subsection. In all cases the cell width is $L = 2\,\mu$m. For these dimensions, a uniform finite element mesh consisting of 80×40 elements is used. Convergence studies have been performed to make sure that this mesh can resolve the heterogeneities in the solution. The simulations start from a stress free state at a temperature of $T_0 = 600$K and cooling is imposed at a rate of $\dot{T} = 4 \times 10^7 \text{K s}^{-1}$. This is an unrealistically high cooling rate but the same as used in the dislocation simulations by Nicola *et al.* (2003a), in order to facilitate comparison.

There are two slip systems in the film, which are oriented at $\varphi^{(1)} = 60^\circ$ and $\varphi^{(2)} = 120^\circ$ degrees from the x_1 axis. To study the effect of slip systems orientation we also model a film having slip systems oriented at $\varphi^{(1)} = 30^\circ$ and $\varphi^{(2)} = 150^\circ$. These orientations differ by a 90° rotation and have the same magnitude of the Schmid factor. Irrespective of the orientation, the film is taken to be elastically isotropic, with Young's modulus $E = 70$GPa, Poisson's ratio $\nu = 0.33$ and thermal expansion coefficient $\alpha_f = 23.2 \times 10^{-6} K^{-1}$. These values are representative for aluminium. For the thermal expansion coefficient of the substrate we take a value correspondent to silicon, $\alpha_s = 4.2 \times 10^{-6} K^{-1}$. Thus, the effective thermal expansion coefficient of the film, used in the calculations, is $\alpha = 19 \times 10^{-6} K^{-1}$.

Consistent with the plane-strain condition, only edge dislocations are taken into account with their Burgers vector in the x_1-x_2 plane. The magnitude of the Burgers vector is $b = 0.25$nm for all dislocations. The drag coefficient is taken to have the value $B = 10^{-4}$Pa s. In discrete dislocation simulations, new dislocations are generated from discrete sources distributed in the film. In the present continuum theory, sources are represented through the production term f as specified by (6.10) with a uniform density $\rho_{\text{nuc}} = 60\ \mu\text{m}^{-2}$ for every slip system. The source strength τ_{nuc} at each integration point is chosen randomly from a Gaussian distribution with mean value $\bar{\tau}_{\text{nuc}} = 25$MPa and standard deviation $\Delta\tau_{\text{nuc}} = 5$MPa separately for each slip system. The nucleation time is taken to be $t_{\text{nuc}} = 10^{-8}$s for all sources and $L_e = 6b$. All the values of the material parameters are identical to those of discrete dislocation plasticity simulations of Nicola *et al.* (2003a).

Besides the material parameters, the nonlocal continuum theory has a few fitting parameters: the coefficient D in the back stress (6.8); the annihilation coefficient A; and the slip resistance τ_{res}. The values of these parameters have been fitted by Yefimov *et al.* (2004a) to discrete dislocation simulations of shearing of a two-dimensional composite material in single slip; the same values were used subsequently in other single and multiple slip problems (Yefimov *et al.*, 2004b; Yefimov and Van der Giessen, 2004c). In the present study we employ the values $A = 5$ and $D = 1$ according to Yefimov *et al.* (2004a), while we choose a value of 7.5 MPa for τ_{res} rather than 15MPa as in the previous studies. The reason for taking the two times smaller value of the slip resistance is that the mean nucleation strength $\bar{\tau}_{\text{nuc}}$ here is also two times smaller than in the previous studies.

6.4.1 Effect of slip orientation

Figure 6.4 shows distinct dependence of the material response upon slip plane orientation in the film crystal. The overall response to cooling, shown in Fig. 6.4a, is presented in terms of the film-average stress parallel to the interface, σ_{11}^{ave}, defined by

$$\sigma_{11}^{\text{ave}} = \int_0^h \int_0^L \sigma_{11}(x_1, x_2)\, dx_1 dx_2 \,.$$

The corresponding plots of the total dislocation density, $\rho_{\text{tot}} = \rho^{(1)} + \rho^{(2)}$, accumulated on both slip systems are shown for the two films in Fig. 6.4b.

Prior to the first nucleation event, the resolved shear stress is uniform and has the same absolute value for both slip systems, either $(60°, 120°)$ or $(30°, 150°)$. Both films have the same distribution of sources and, therefore, start to yield at the same temperature $T_{\text{Y}} = 591$K, as seen in Fig. 6.4a. After initial yield, starting at approximately $T = 585$ K the film with $(60°, 120°)$ slip systems exhibits a harder response than the other film with 30° and 150° slip systems. The latter film shows very little overall hardening and apparently requires less dislocation activity to relax the stress, as seen in Fig. 6.4b.

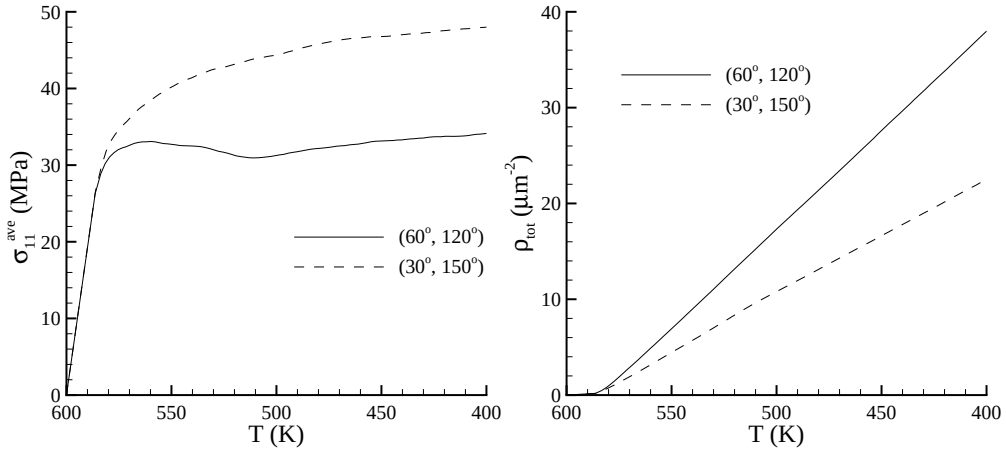

Figure 6.4 Effect of slip system orientation on (a) stress-temperature curve and (b) evolution of accumulated total dislocation density $\rho_{\text{tot}} = \rho^{(1)} + \rho^{(2)}$ with temperature.

It should be noted that the nonlocal theory predicts a nonlinear type of hardening from initial yield at $T = 591K$ down to approximately $T = 500K$. This finding is somewhat at odds with the discrete dislocation results of Nicola *et al.* (2003a) which suggest a linear hardening on average during the whole cooling process. However, as cooling goes on further from $T = 500K$, the hardening rate in the nonlocal plasticity simulations remains nearly constant and equal to that predicted by the discrete dislocation simulations. Although we have not been able to exactly

trace the origin of the initial nonlinear hardening, we suspect it has to do with the nonlocal interaction law (6.7) between slip systems; as discussed before, this interaction law is fully phenomenological and chosen on the basis of a comparison for simple shearing. We have checked that it is not a coincidental result for the chosen nucleation distribution, by repeating the calculations with other random ones. The responses were all practically identical to the one shown in Fig. 6.4a.

The accumulated total dislocation density in both films increases linearly with temperature as seen in Fig. 6.4b. Figure 6.4b also shows that the density in the film with $(60^\circ, 120^\circ)$ slip systems differs from that in $(30^\circ, 150^\circ)$ film by a factor $\cos 30/\cos 60$, which is consistent with the dislocation-based stress relaxation mechanism proposed by Nicola *et al.* (2004a) in their study of hardening mechanisms in single crystal thin films.

The dislocation structure, reflected in the distribution of the ρ field, that has been formed in the film at the end of the cooling process is depicted in Fig. 6.5 for the two crystal orientations. The model predicts the formation of a distinct layer at the bottom surface of the each film, densely populated by dislocations, while in the rest of the film the dislocation density is significantly lower. The spatial fluctuations in the dislocation density are to be attributed to the random distribution of source properties. The width of the dislocation layer in both films is less than 0.1μm but it is slightly larger for the $(60^\circ, 120^\circ)$ film. These finding are consistent with the discrete dislocation plasticity study of Nicola *et al.* (2003a).

The formation of the boundary layer is triggered by the dislocations that move towards the bottom surface of the film and pile-up against the impenetrable wall at $x_2 = 0$. From the distribution of the net-Burgers vector densities in the $(60^\circ, 120^\circ)$ film shown in Fig. 6.6, it is seen that positive dislocations of slip system 1 and the negative ones on the slip system 2 dominate. The corresponding opposite sign dislocations from the two slip systems have left the film through the top surface. Figure 6.6 also reveals that the two slip systems contribute approximately equally to the boundary layer since $|k^{(1)}| \approx |k^{(2)}|$ everywhere. Since the densities on the two slip systems are also roughly the same, it follows from comparison of Fig. 6.6 with Fig. 6.5(a) that almost all dislocations are geometrically necessary. A dislocation structure similar to that in Fig. 6.6 has been found in the $(30^\circ, 150^\circ)$ film and is therefore not shown.

Dislocation nucleation and motion lead to stress relaxation in the core of the film. The near-interface region, where plasticity is hindered, remains stressed, and high back stresses are created by the dislocation pile-ups in the dislocation layer represented by the gradients in the $k^{(\beta)}$ fields. Distributions of the in-plane stress σ_{11} are shown in Fig. 6.7 for the two films after cooling down to $T = 400$K. The stress is normalized by the elastic stress

$$\sigma_{\rm n} = \frac{E}{(1-\nu)}\alpha(T - T_0), \tag{6.20}$$

which would be present in the film if plastic relaxation had not occurred. For the set of parameters employed in this study, $\sigma_{\rm n} = 397$MPa. According to Fig. 6.7 the stress distribution is qualitatively insensitive to the crystal orientation. The width of the highly stressed layer seems to be correlated with the boundary layer thickness in each of the two films. Quantitatively, the

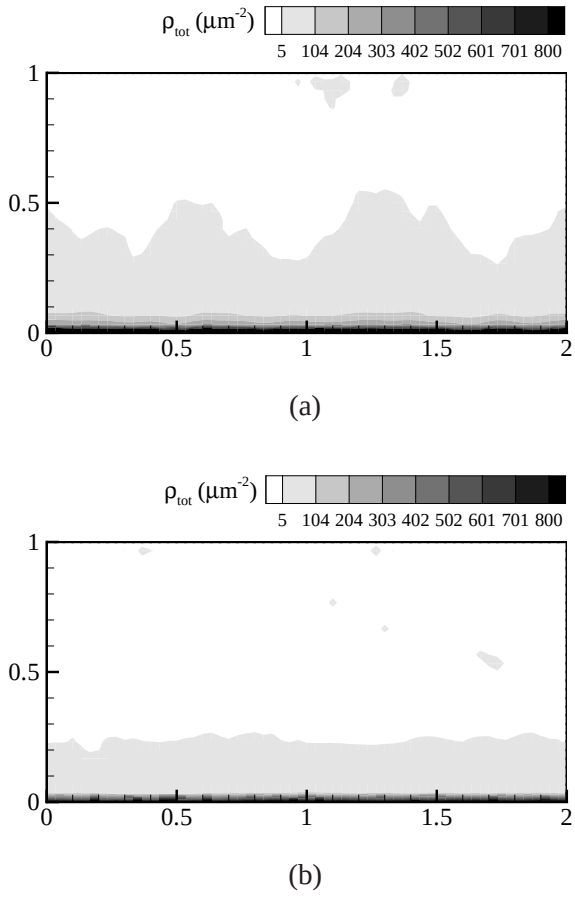

Figure 6.5 Distributions of the accumulated total dislocation density $\rho_{tot} = \rho^{(1)} + \rho^{(2)}$ for the case (a) (60°, 120°) and (b) (30°, 150°) at the end of cooling, $T = 400$K.

core region is more relaxed and the highly stress boundary layer is thinner in the (30°, 150°) film than in the one with (60°, 120°) slip systems. These two features give rise to an overall softer response of the (30°, 150°) film that was shown in Fig. 6.4.

6.4.2 Size effects

To analyze the influence of size on the material response, we perform calculations for various film thicknesses. Figure 6.8 compares the results for films having thicknesses $h = 0.5\mu$m, 1μm or 2μm for two slip systems at $\varphi^{(1)} = 60°$ and $\varphi^{(2)} = 120°$. The size effect for the same thicknesses but for slip systems at 30° and 150° is shown in Fig. 6.9.

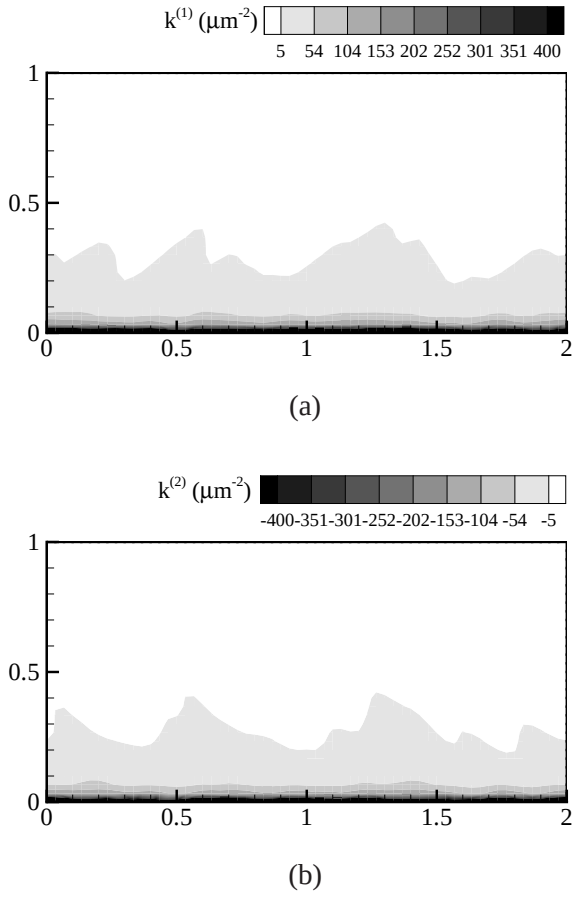

Figure 6.6 Distributions of the sign-dislocation density k for (a) the slip system 1 ($\varphi^{(1)} = 60°$) and (b) for the slip system 2 ($\varphi^{(2)} = 120°$) at $T = 400K$.

Figures 6.8a and 6.9a display the systematic trend that the hardening rate increases with decreasing film thickness, independent of the slip system orientation. For all cases analyzed the first nucleation process occurs at the same temperature of $T = 591K$, since it is controlled by the strength of the weakest dislocation source and the Schmid factor. The stress strain response for the films of all sizes shows no size effect until the films are cooled down to approximately $T = 585$ K and a stress level of 30MPa is reached. Upon further cooling, the response of a $(30°, 150°)$ film of any h is seen to be softer than that of the film with $(60°, 120°)$ systems of the same thickness. The accumulated total dislocation densities increase linearly with temperature in all cases analyzed, Figs. 6.8b and 6.9b. The total density decreases with increasing film thickness, roughly speaking, because most dislocations are located in the boundary layer, noticed before

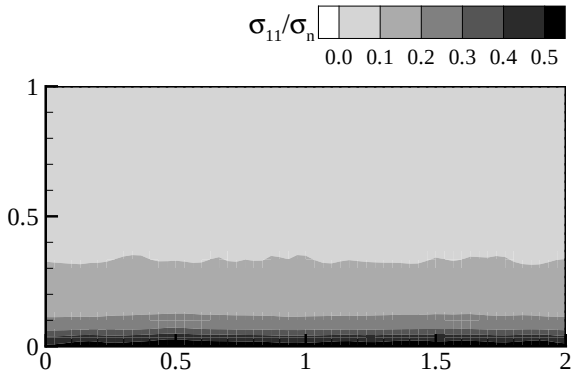

(a)

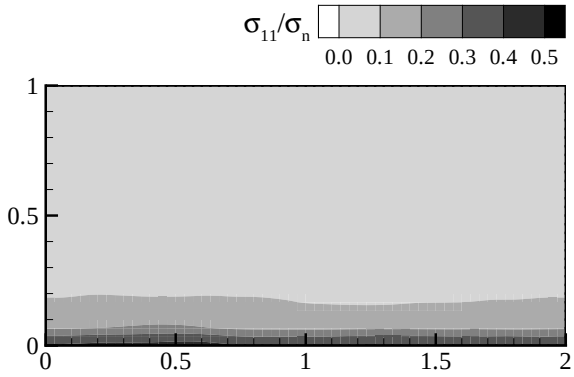

(b)

Figure 6.7 Distribution of σ_{11} normalized by σ_n for the films with two slip systems: (a) (60°, 120°) and (b) (30°, 150°) after cooling down to $T = 400$K.

in Fig. 6.5, whose thickness does not scale with the film thickness.

The size-dependence of the overall response originates from the boundary layer being highly stressed. This effect can be seen in Fig. 6.10, where the through-thickness profile of the in-plane stress $< \sigma_{11} > (x_2)$, averaged over the x_1 direction, i.e.

$$< \sigma_{11} > (x_2) = \frac{1}{L} \int_0^L \sigma_{11}(x_1, x_2)\, dx_1 \,, \tag{6.21}$$

is plotted for three values of the film thickness and for both orientations. The total averages σ_{11}^{ave} in the films are also shown for comparison. The stress profiles clearly show that the contribution of the boundary layer to the film average stress is largely independent of film thickness. It is also seen that for the $(60°, 120°)$ films the stress inside the layer is at least three

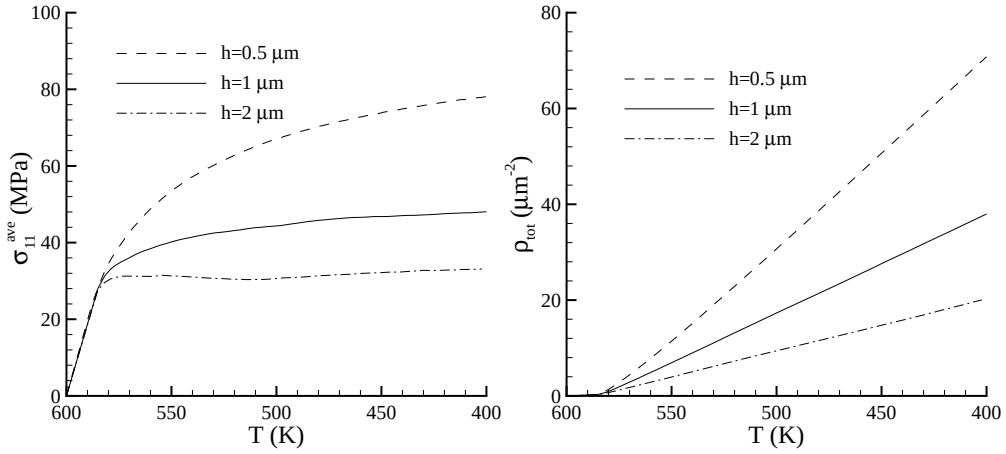

Figure 6.8 Effect of film thickness *h* on (a) stress–temperature response and (b) evolution of the ρ_{tot} density versus temperature for slip systems $(60°, 120°)$.

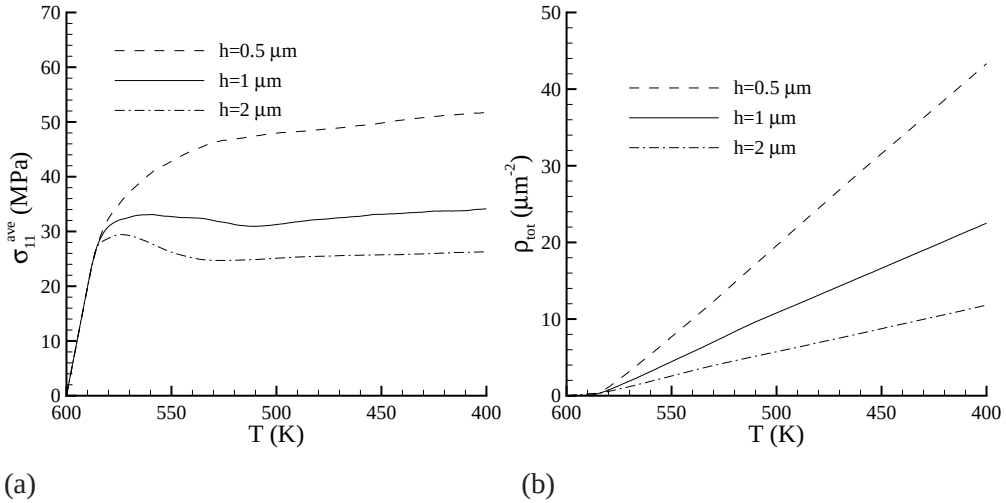

Figure 6.9 Effect of film thickness *h* on (a) stress–temperature response and (b) evolution of the ρ_{tot} density versus temperature for slip systems $(30°, 150°)$.

times higher than the total averaged stress. Although the stresses in the boundary layer are much higher than those in the relaxed part of the film, the main contribution to the total stress originates, however, from the relaxed part of the film. A similar conclusion holds for the $(30°, 150°)$ film but the difference between the total average and the stress levels in the boundary layer is somewhat smaller.

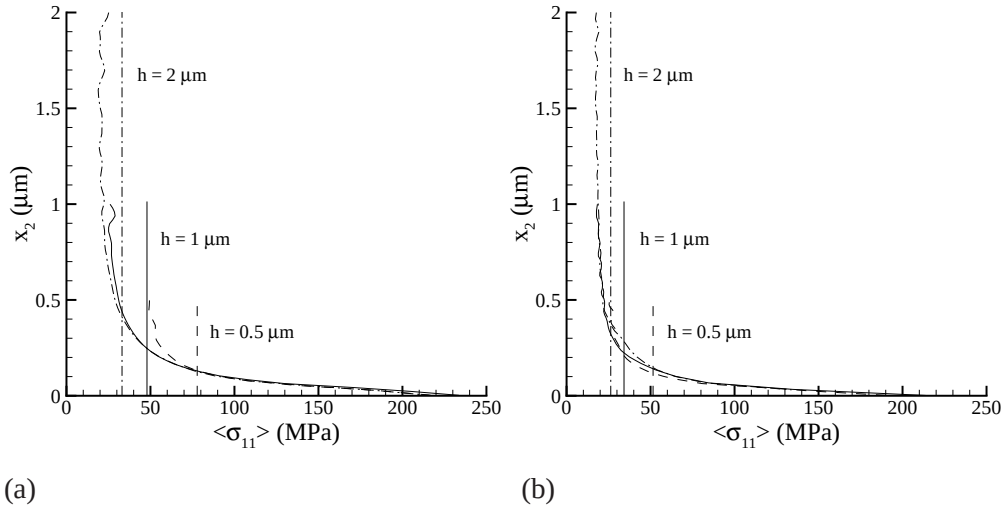

Figure 6.10 Profiles of $< \sigma_{11} > (x_2)$ for different film thicknesses in (a) $(60°, 120°)$ film and (b) $(30°, 150°)$ film at 400K. The vertical lines denote the corresponding film averages σ_{11}^{ave}.

6.5 Conclusion

We have studied stress relaxation in thin films by means of the recently formulated nonlocal crystal plasticity theory (Yefimov and Van der Giessen, 2004c). The multiple-slip model used here is a generalization of the single-slip theory (Yefimov *et al.*, 2004a) which is founded on a rigorous statistical-mechanics treatment of the behavior of an ensemble of edge dislocations on parallel glide planes by Groma (1997). The only approximation made in the derivation concerns the correlation function between dislocations. The natural length scale that emerges from the derivation is the mean dislocation spacing $1/\sqrt{\rho}$. While a truly multiple slip analysis is underway (cf. Zaiser *et al.*, 2001) but not ready, we have simply generalized the single-slip theory to multiple slip systems and checked it against discrete dislocation simulations for the confined shearing of a single crystalline strip (Yefimov and Van der Giessen, 2004c).

The numerical solution of the addressed thin film problem has been obtained by applying the finite elements method and using the parameter values determined in the previous studies of the nonlocal theory (Yefimov *et al.*, 2004a, b; Yefimov and Van der Giessen, 2004c) for the same material. No additional fitting has been done. Nevertheless, the predictions are in quite good agreement with discrete dislocation plasticity results. The nonlocal theory has been shown able to pick up the orientation dependance of the overall stress vs. temperature response, the formation of a boundary layer of dislocations at the film-substrate interface and the associated size effect. All these findings give further confidence in the interaction law (6.7) governing the contribution of back stress generated on one slip system onto another one. It should be emphasized, however, that this interaction law does not rest on solid grounds and that better

versions are likely to be possible.

The present work supplements other nonlocal continuum plasticity studies of thin films. Gudmundson (2004) has given a closed-form solution of the same problem using his own strain gradient theory. The latter belongs to a class of phenomenological strain gradient theories for crystal plasticity that incorporate a length scale via the dependence of plastic flow on the dislocation density tensor. The latter is Nye's (1953) representation of geometrically necessary dislocations. In both Gudmundson's (2004) and Gurtin's (2002) theory, the dislocation density tensor enters through an additional contribution to the free energy. Gurtin's original proposal for this defect energy function was used in (Nicola *et al.*, 2003b), but was found to be unable to pick up the orientation dependence discussed for the present theory in Sec. 6.4.1. A few new energy functions have been proposed and studied very recently (Nicola *et al.*, 2004b).

It is emphasized that the class of phenomenological strain-gradient theories mentioned in the previous paragraph share the property that the material length scale is constant, whereas in the present theory it is an evolving quantity. Also, among the theories mentioned explicitly, the present theory has so far proved to be the only one that, with the same set of material parameters, can capture the behaviour of diverse boundary-value problems such as shearing of a composite, bending, shearing of constrained layer and thin films.